ODS FeCrAl Alloys

Subjects: Materials Science, Characterization & Testing

Contributor: Xi Wang , Xinpu Shen

After the Fukushima nuclear accident, the development of new accident-tolerant fuel cladding materials has become a research hotspot around the world. Due to its outstanding corrosion resistance, radiation resistance, and creep properties at elevated temperatures, the oxide dispersion strengthened (ODS) FeCrAl alloy, as one of the most promising candidate materials for accident-tolerant fuel cladding, has been extensively studied during the past decade. In particular, the reasonable/optimized content of Cr is explained from the aspects of oxidation resistance, radiation resistance, and thermal stability. The essential role of the Al element in oxidation resistance, high-temperature stability, and workability was reviewed in detail. The roles of oxide-forming elements, i.e., Y (Y_2O_3), Ti, and Zr, and the solid solution strengthening element, i.e., W.

ODS FeCrAl | accident-tolerant fuel cladding | oxidation resistance

1. Introduction

Since the beginning of the new century, with the continuous growth of global power demand and the dual challenges of energy shortage and environmental protection, countries all over the world have paid more attention to nuclear energy compared with fossil energy. As the most promising alternative to fossil energy, nuclear energy is considered a clean energy source with low carbon emissions and high efficiency. Nuclear power generation has a history of more than 60 years. However, due to the deep negative impact of nuclear accidents on human beings and the environment, the safety of nuclear energy has become the focus of attention around the world. For example, in the 1990s, after the accidents at the Three Mile Island and Chernobyl nuclear power plants, the United States, Europe, Japan, and other countries researched and tackled key issues actively for the development of the derived third generation reactors to prevent and mitigate serious accidents. Compared to the second-generation nuclear power units where the Fukushima nuclear accident in Japan (11 March 2011) occurred, the safety and economy of the current mainstream third-generation nuclear power units have been significantly improved. One of the measures is to adopt a material combination different from the existing zircaloy-clad-UO_2 fuel system but possessing the same operating performance (burnup, power grade, abundance) as it, which aims to improve accident tolerance by transitioning from a zirconium-based fuel cladding to an excellent oxidation-resistant cladding material in the light water reactor (LWR). Although the course of the accident in LWR is controlled by the reaction of the entire (cladding-fuel) system during the accident, the accident-tolerant cladding material can significantly influence the rate of the process and consequences of the accident, which is very important to minimize the burden on the safety systems and maximize the response time. In this case, the safety margin of the nuclear power system can be improved [1]. In addition, the development of the accident-tolerant cladding is also a key issue for the high burnup operation of IV generation nuclear power system, such as the Supercritical Pressurized Water

Reactor (SPWR) and the Lead Bismuth-Budding Fast Reactor (LFR). In particular, after the severe accident at Fukushima Nuclear Power Plant, nuclear reactor designers realized the importance of improving safety margins in severe accidents, and the U.S. Department of Energy started a research project on accident-tolerant fuels (fuels and fuel claddings) [2][3][4][5][6][7][8][9].

It is well understood from this extensive field of research that optimal oxidation resistance is usually achieved by forming Cr_2O_3, Al_2O_3, or SiO_2 layers above 600 °C in air on the surface of structural materials or coatings containing Cr, Al, and Si elements [10]. Therefore, coated zirconium-based cladding, ferritic alumina-forming alloy cladding, and silicon carbide fiber-reinforced silicon carbide matrix composite cladding are considered to be the main candidates for cladding materials for accident-tolerant fuel claddings [11]. According to the research results of dry air exposed for longer than 1000 h, Cr_2O_3 can provide protection up to 1000 °C, Al_2O_3 up to 1400 °C, and SiO_2 up to 1700 °C (the exact upper limit temperature depends on multiple factors, such as component thickness, exposure conditions, and expected life). However, under severe accident conditions, the environment inside the reactor core may consist of steam or a mixture of steam and hydrogen. In the elevated temperature environment with steam, the Cr_2O_3 and SiO_2 oxide scales can form volatile hydroxides, which can reduce their service limit at high temperatures by several hundred degrees compared with the temperature limit in dry air [12]. The oxidation resistance of SiC-based materials and stainless steel supplemented with high chromium and/or aluminum was tested at temperatures ranging from 800 °C to 1200 °C in a high-pressure steam environment. The results showed that the FeCrAl alloys exhibited very low reaction kinetics up to 1200 °C; however, the Fe–Cr alloys with 15–20 wt.% Cr were corroded at a relatively high rate [13]. Thus, from the viewpoint of corrosion resistance at ultra-high temperatures (T > 1000 °C), FeCrAl-based alloys are considered to be the most desirable candidates as accident-tolerant fuel cladding in light-water nuclear reactors.

The fuel cladding is the shell to seal the nuclear fuel, serving as the most important safety barrier for nuclear power plants. Its main function is to prevent the escape of fission products, prevent the fuel from being corroded by coolant, and effectively export thermal energy. Due to the extreme service conditions of nuclear reactors, the fuel cladding is confronted with extremely high burn-up temperatures, strong radiation doses, and compatibility issues with the coolant. The fuel cladding material needs to have excellent comprehensive performance to overcome challenges such as:

(1) High thermal conductivity, low coefficient of thermal expansion;

(2) Small neutron absorption cross-section, low induced radioactivity, short radioactive half-life, and good radiation resistance;

(3) Good compatibility between the fuel and the coolant (strong corrosion resistance);

(4) High strength, good plasticity, and toughness at elevated temperatures.

Therefore, the design of chemical composition is one of the key measures for alloys to meet the service requirements of nuclear reactors.

Oxide dispersion strengthened (ODS) alloys have a strong pinning effect on the movement of dislocations and grain boundaries due to the ultra-high density dispersed nanosized oxides [14][15][16], which can significantly improve the high-temperature strength of the material [17]. High-density nanosized oxides can also promote the recombination of point defects caused by irradiation, including the recombination of vacancies and self-interstitial atoms, reducing radiation damage [18]. Due to their excellent radiation resistance and excellent high-temperature strength, ODS alloys are considered candidate materials for fast reactor fuel cladding and the first wall/cladding of a fusion reactor.

The ODS FeCrAl alloy combines the prime mechanical properties at elevated temperatures [19][20] and the radiation resistance [21][22][23][24][25] of the ODS Fe–Cr alloy with the optimized corrosion resistance of the FeCrAl alloy. Thus, it is considered a very promising candidate for solving the issue of accident-tolerance structural materials applied in nuclear energy systems, especially for the II and III generations of Lightwater Reactors (LWRs), the IV generation of Supercritical Pressurized Water Reactors (SCPWs), and Lead-Cooled Fast Reactors (LFR, using liquid lead alloy as coolant) [26][27].

The roles of matrix elements (Cr/Al), oxide–forming elements (Y_2O_3/Ti/Zr), and solid solution strengthening element (W) in the ODS FeCrAl alloy were discussed. The effects of Cr on corrosion resistance, irradiation resistance, thermal stability, microstructure, and mechanical properties were summarized. The critical roles of Al in corrosion resistance at different conditions were reviewed in more detail. The effect of Al on the strength and workability of the ODS FeCrAl alloy were discussed in an independent section. Moreover, the upper limits of their contents were also explained on the basis of the several constraints above. The typical types of oxide, i.e., Y–Ti–O phase, Y–Al–O phase, and Y–Zr–O phase, and their formation mechanisms in alloy systems were introduced in detail. All aspects mentioned above are of reference significance for understanding the development of the ODS FeCrAl alloy for the tolerance of accidents in nuclear applications from the perspective of composition design. **Figure 1** displays the frame diagram, which briefly outlines the considerations of chemical composition design.

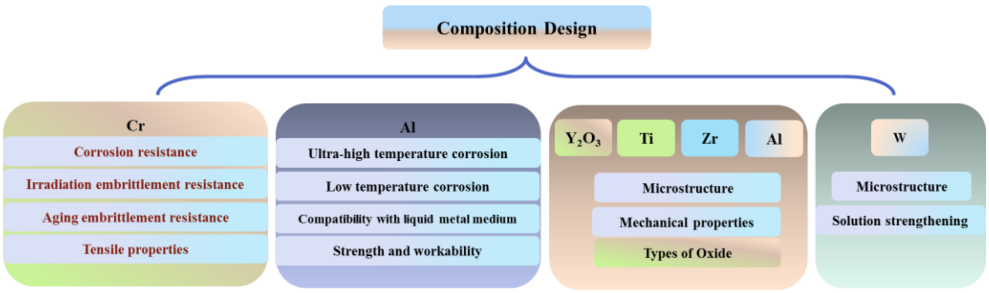

Figure 1. Frame diagram of composition design.

2. Effect of Chemical Elements on the Properties and Microstructure of ODS FeCrAl

Alloying composition or content design depends on multiple constraints in nuclear applications, such as radiation resistance, corrosion resistance, high-temperature strength requirements, processing feasibility, etc. Thus, taking

measures of balancing and adjustment in the aspect of chemical composition design has always been an important part of the research and development of nuclear-level ODS FeCrAl. The effects of chemical elements such as Cr, Al, Y_2O_3, Ti, Zr, and W are discussed in the following content. Particularly, considering that the cladding material operates in the actual environment of SCW and LBE fission reactors with radiation and corrosive medium for the long term, it should be emphasized that Cr and Al content are determined mainly according to the results of corrosion and radiation tests [28].

2.1. The Influence of Cr

For Al-free ODS Fe–Cr alloys, increasing the content of Cr can improve their corrosion resistance, according to the experimental results. Pint et al. [29] compared the corrosion resistance of four ODS 13–14 at.% Cr iron base alloys in air and 10 vol.% water vapors for 10,000 h at 700–1100 °C. The results showed that the reaction rates of all ODS alloys are lower than those of stainless steel (type 347 stainless steel (18 wt.% Cr), type 310 stainless steel (25 wt.% Cr), and NF709 (Fe–20Cr–25Ni–Nb) at 700–800 °C. However, the limit temperature of alloys with a low Cr content in air is 900 °C. However, studies on ODS alloys containing 21 wt.% Cr (high content) showed that they have good oxidation resistance up to 1100 °C due to the formation of a coherent and Cr-rich oxide film [30]. Studies that refer to increasing Cr content as improving the corrosion resistance of alloys in the SCPW (783 K, 25 MPa) environment were also reported [31][32]. For example, Kimura et al. [31] concluded that in SCPW, an increase in Cr concentration to 16 wt.% significantly increases the corrosion resistance of ODS ferritic steels. Cho et al. [32] demonstrated that the higher the Cr concentration, the fewer Fe–Cr-rich corrosion products there are and the better the corrosion resistance of ODS steel when exposed to high–Cr ODS alloys in SCPW. However, the service temperature in the nuclear reactor ranges from 300 to 650 °C, and cladding material with a Cr element of 14–22 wt.% undergoes aging hardening during long thermal aging, which is called “475 °C embrittlement” [33][34][35][36]. Lee et al. [37] studied the effect of thermal aging (for 1000 h at 430–475 °C) on the microstructure and mechanical properties of ODS alloys with a high Cr content ranging from 14 to 22 wt.% by TEM, microhardness, and small punching (SP) tests. The SP-ductile to brittle transition temperature (SP-DBTT) and microhardness of ODS steel after aging increased significantly with changes in Cr content, aging time, and temperature due to the formation of the Cr–α′ rich phase.

In terms of irradiation stability, Field et al. [38] and Briggs et al. [39] reported that high Cr alloys could produce irradiation-induced harmful and embittered Cr–α′ rich phases at 300–350 °C. Therefore, commercial high-Cr ODS alloys, such as PM2000 and MA956, are not classified as nuclear-grade alloys due to aging and irradiation-induced embrittlement, although they were manifested to have satisfactory corrosion resistance. However, under moderate temperature irradiation, the reduction of Cr content hinders the formation of an embittered Cr–α′ rich phase, which can avoid damage to mechanical properties due to α′–α in the corresponding service environment [38][39]. Fortunately, the change in Cr content has no significant effect on the mechanical properties [40][41]. For example, Li et al. [40] compared three kinds of ODS alloys containing different Cr contents, i.e., Fe–12Cr–0.5Ti–1.0W (Alloy A), Fe–16Cr–0.5Ti–1.0W (Alloy B), and Fe–18Cr–0.5Ti–1.0W (Alloy C) alloys (all in wt.%). Regarding the important mechanical properties, such as tensile strength, hardness, and impact toughness, it was found that there was no linear proportional relationship between Cr content and mechanical properties on the ODS Fe–Cr alloys, as shown

in **Figure 2**. Noh et al. [41] also concluded that Cr was the most important element in determining the matrix phase and that there was no significant influence on the tensile properties of ODS steel at 700 °C. Therefore, it is feasible to adjust the content of Cr to not only maintain the bcc matrix phase but also to avoid the emergence of a harmful brittle phase without damaging the mechanical properties.

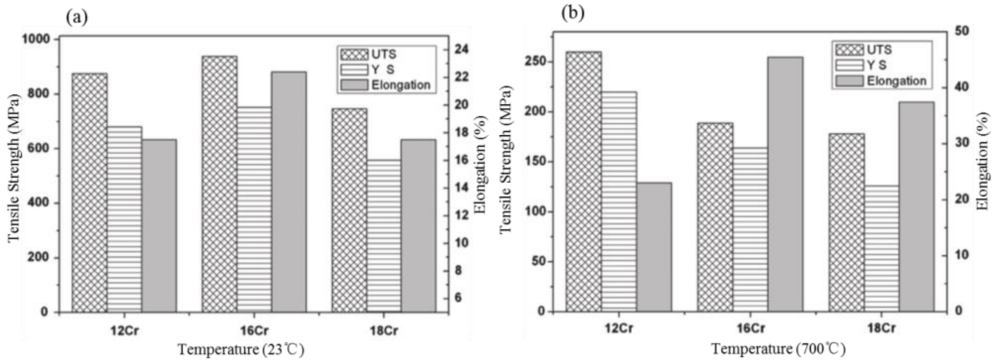

Figure 2. A comparison of tensile strength and elongation of different specimens at RT and 700 °C: (**a**) Low magnification image, (**b**) High magnification image.

As summarized above, too high a Cr content has led to many unfriendly trends in the performance of the ODS alloy, as shown in **Figure 3**. Therefore, reduction of Cr content is an essential measure based on the considerations of high-temperature irradiation in nuclear reactor applications [42][43][44], and an Al element is added to the ODS Fe–Cr alloy to compensate for the lack of corrosion resistance of the alloy.

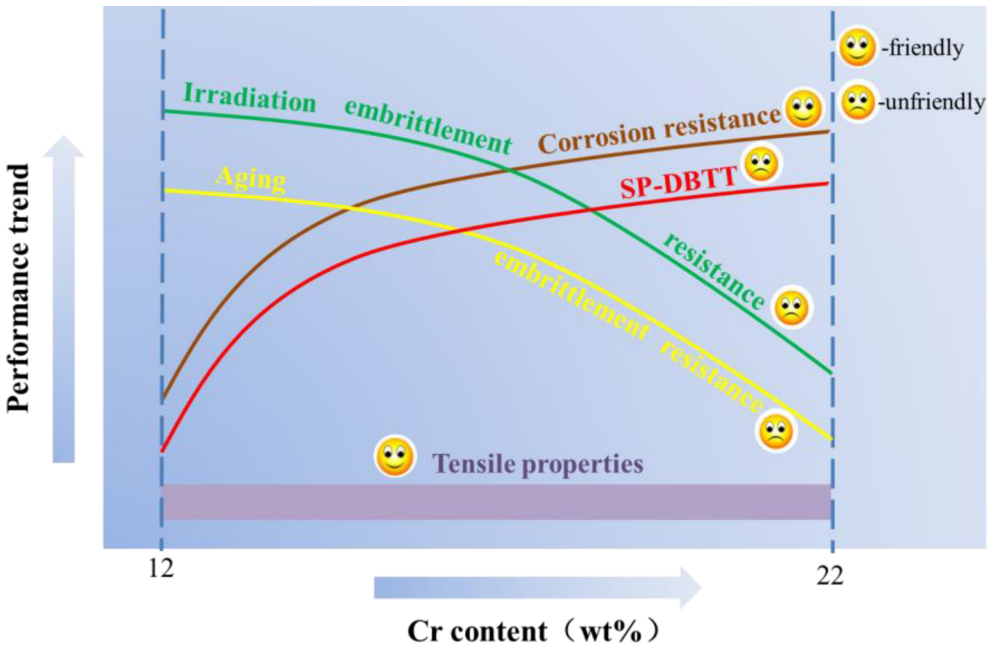

Figure 3. Schematic diagram of the trend of properties changing with Cr content.

2.2. The Influence of Al

In order to balance the weakening of corrosion resistance caused by the reduction of Cr content and considering that Al_2O_3 scales can withstand high temperatures up to 1400 °C to protect the underlying matrix effectively, an appropriate amount of Al addition was added to ODS Fe–Cr alloys to produce an Al–rich oxide film (Al_2O_3) with better performance than Cr–rich oxide film in the case of an accident. In addition, the Cr element can assist in the formation of the Al_2O_3 scale, that is, the third element effect. For example, Niu et al. [45] systematically studied the oxidation behavior of Fe–x Cr–3 at.% Al alloy (x = 2, 3, 5, and 10 at.%) at 1000 °C. It was found that the presence of a third element, Cr, promoted the formation of an Al_2O_3 oxide layer [46] in alloys with low Al concentrations. Meanwhile, the synergy effect between Cr and Al is also reflected with respect to the suppression of 475 °C embrittlement by Al addition. In terms of previous experimental observations, Kobayashi and Takasugi [47] discovered that the suppression of 475 °C embrittlement due to Al addition could be attributed to the inhibition of the nucleation of α′ phase. Regarding the simulation calculation, Li et al. [48] studied the effect of Al addition on the formation energy of the α–α′ interfaces in Fe–Cr alloy systems by utilizing the first-principles theory and suggested that Al reduced the stability and affected the formation energies of the α′ phase, resulting in suppression of phase separation in Fe–Cr alloy systems by adding Al. Theoretically, the Fe–Cr–Al ternary diagram [49] can be used as a guiding basis to prevent the generation of α′ phase with respect to chemical composition design. **Figure 4** shows the Fe–Cr–Al alloy system, when the content of Cr is fixed, increasing the content of Al can effectively inhibit the generation of α′ phase.

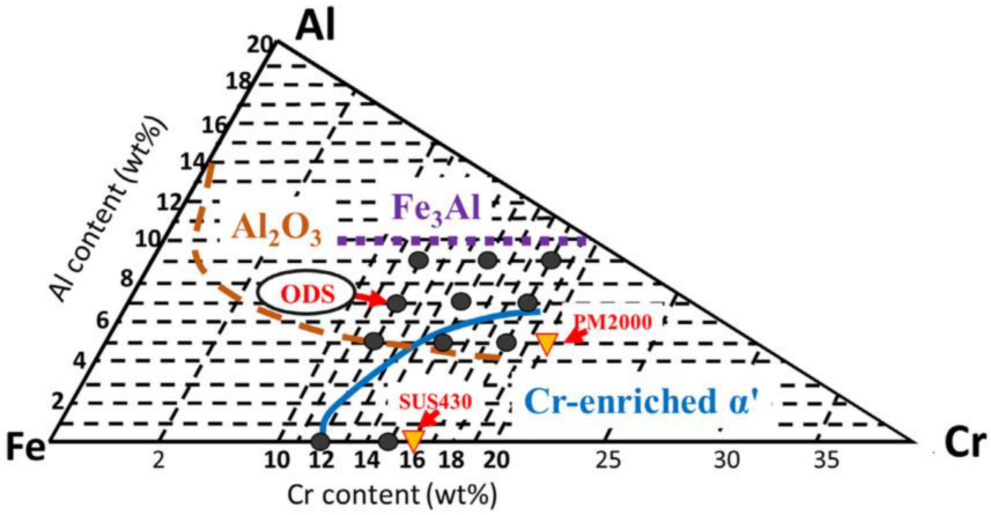

Figure 4. Fe–Cr–Al ternary diagram: black spots and triangles represent the compositions of the ODS steels investigated in the presented work and the commercial steels, respectively. The Al_2O_3 formation zone at 1100 °C is bounded by a broken line. The zones of Fe_3Al and Cr-enriched α phases at 475 °C are bounded by a dotted line and a solid line, respectively.

Recently, some scholars have also verified the effect of the Al element on inhibition of α′ phase [50][51]. For example, Yang et al. [51] characterized α′ phase evolution by the atom probe, which evolved an entire process of nucleation, growth, and coarsening of α′ phase during aging at 475 °C. The results showed that in the case of 15 wt.% Cr, the size of α′ phase in the model alloy containing 4.5 wt.% Al grows gradually with the aging time up to 10,000 h, while

α′ phase in the model alloy containing 6 wt.% Al is effectively suppressed, as shown in **Figure 5**. These experimental observations are in good agreement with the theoretical prediction displayed in **Figure 4**.

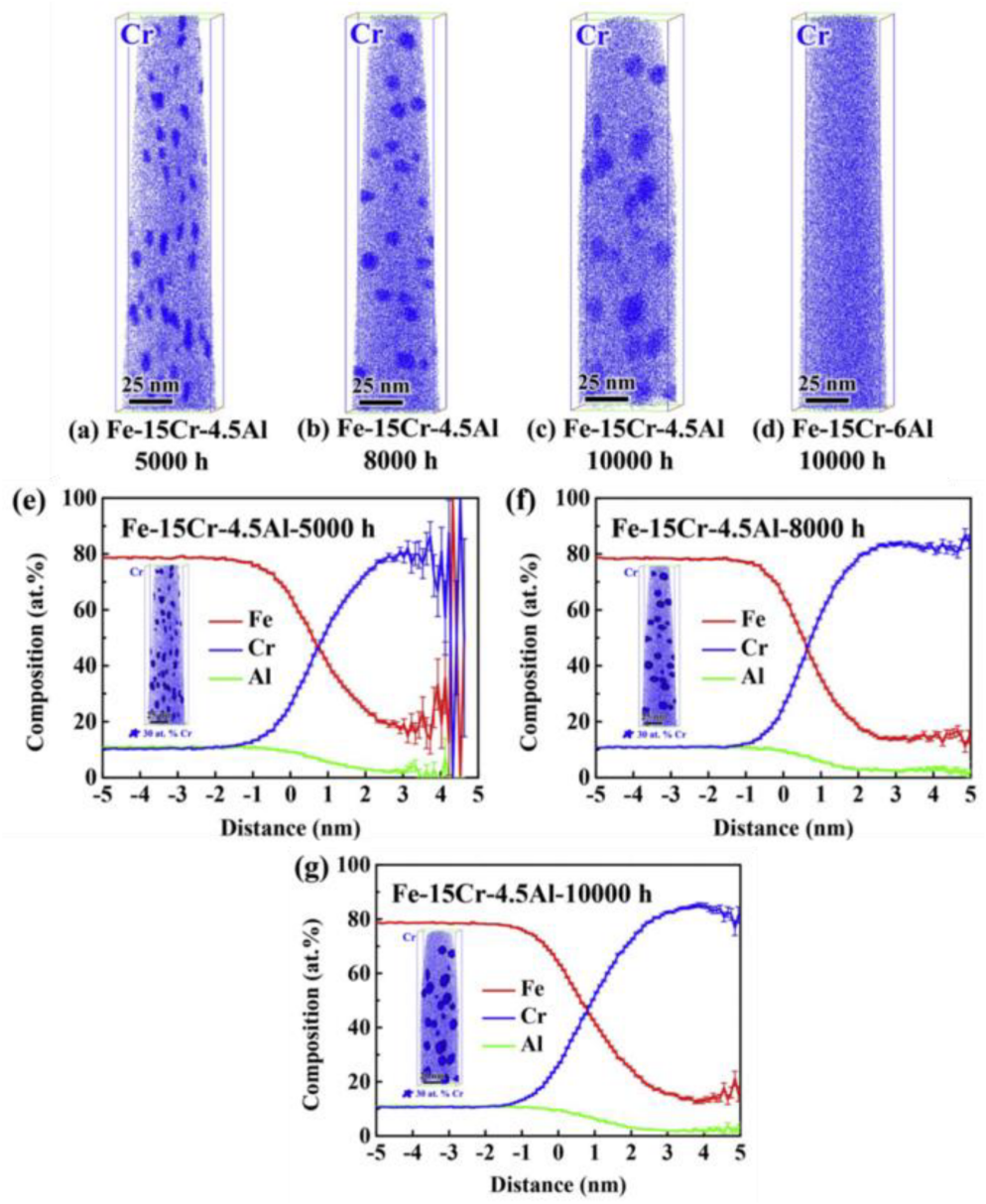

Figure 5. Atom probe maps of Cr for the Fe–15Cr–4.5Al alloy aged at 475 °C for (**a**) 5000 h, (**b**) 8000 h, and (**c**) 10,000 h, as well as (**d**) the Fe–15Cr–6Al alloy aged at 475 °C for 1000 h, 3D atom distributions with Cr iso–concentration surfaces at 30 at.%, and proximity histograms of the α′ phases generated by Cr iso–concentration surfaces of the Fe–15Cr–6Al alloy aged at 475 ◦C for (**e**) 5000 h, (**f**) 8000 h, and (**g**) 10,000 h.

2.2.1. Ultra-High Temperature Corrosion (T > 1000 °C)

As for the high-temperature corrosion studies of the ODS FeCrAl alloy, scientists are most especially concerned about the corrosion behavior of the alloys under simulated accident conditions, i.e., loss-of-coolant accidents (LOCA). To prove the important role of the Al element, the corrosion behavior of the ODS FeCrAl alloy at ultra-high

temperatures up to 1621 °C [52][53]. Liu et al. [54] carried out oxidation tests on six ODS ferritic alloys and SUS430 at 1050 °C for 200 h in air. The results showed that the oxidation resistance of the 14Cr ODS FeCrAl alloy containing Al elements was better than that of SUS430 (16.8Cr). With an increase in Al concentration, the oxidation resistance of the 16Cr ODS alloy was significantly improved from 0 to 2 and 4 wt.%, and the mass gain decreased from 8.6 to 7.6 and 4 g/m^2. The thickness of the Al_2O_3 oxide layers of the 16Cr–4Al ODS alloy can only be 3.5 μm. While ODS alloys containing 11 wt.% Cr and 2 wt.% Al cannot form a dense alumina layer. The concentrations of Al and Cr should be greater than 2 and 14 wt.%, respectively, to form a dense Al_2O_3 layer and enhance adherence between the Al_2O_3 layer and the matrix. The author [55] studied systematically the effect of Al content on the oxidation behavior of $Y_2Ti_2O_7$ dispersed Fe–14Cr ferritic steel in air at 1100 °C for 200 h. It was concluded that in 14CrODS steel containing 14 wt.% Cr, a solid and continuous Al_2O_3 film is formed, and the content of Al is not less than 4.5 wt.%. Furthermore, previous studies also showed that a reduced Cr content and enhanced Al content provide the basis for the formation of a stable and protective Al oxide layer [56][57]. In a Fe–Cr–Al alloy with 1015 wt% Cr, an Al content as low as 3 wt.% is sufficient to form an Al oxide layer. The Oak Ridge National Laboratory (ORNL) in the United States developed the first generation 12Cr ODS FeCrAl alloy (low Cr), and the evaluating experiment started with oxidation performance in simulated accident status at 1200 °C for 4 h in 1 bar dry air or steam. All evaluated components, including 12Cr–5Al, formed a protective film in steam at 1200 °C, while the ODS Fe–14Cr alloy did not form a protective oxide film under the same experimental conditions, and metal consumption was 50% after 8 h in this environment [58][59]. Subsequently, in order to improve the ductility of the alloy, the second-generation Fe–(10–12)–Cr–6Al ODS alloys with a low O content and 0.15–0.5 wt.% Zr were derived from the first-generation low Cr12–15Cr ODS FeCrAl alloy in ORNL. The experimental results of the isothermal oxidation test up to 1400 °C in air or steam showed that this series of alloys have excellent corrosion resistance above 1200 °C under simulated accident conditions, as shown in **Figure 6** [60].

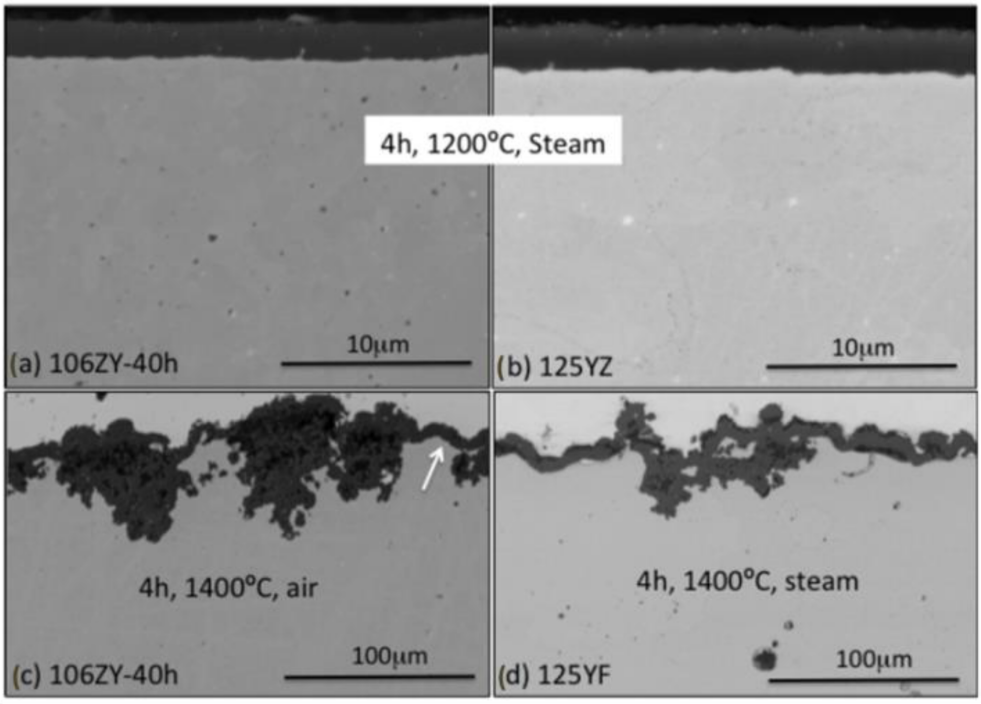

Figure 6. BSE-SEM micrographs of the oxide scale formed (**a**) after 4 h at 1200 °C in steam, alloy 106ZY 40 h; (**b**) after 4 h at 1200 °C in steam, alloy 125YZ; (**c**) after 4 h at 1400 °C in air, alloy 106ZY 40 h; (**d**) after 4 h at 1400 °C in steam, alloy 125YF. The scale bars for (**c**,**d**) are ten times larger than the scale bars for (**a**,**b**). The white arrow highlights an area where the scale is locally protective.

Qiao et al. [61] calculated the corresponding Gibbs free energy of different oxide layers at 1200 °C by Fact Sage. The priority order of each element that forms oxides in the Fe–Cr–Al alloy can be predicted as Al_2O_3 > Cr_2O_3 > $FeCr_2O_4$ > Fe_2O_3 > FeO > Fe_3O_4, thus Al will take precedence over Cr and Fe oxidation, which is consistent with previous experimental results.

Regarding oxidation resistance studies under simulated accident conditions, the research team of Hokkaido University in Japan evaluated systematically the oxidation behavior of a series of the ODS 15Cr–7Al alloys in air and steam at 1200–1500 °C, simulating the LWR severe accident together with analyses using the thermochemical multiphase computer software FactSage (https://www.factsage.com/, 11 September 2023). Additionally, they found that the alumina scale formed on the ODS FeCrAl alloy with an appropriate composition can maintain good adhesions up to 1400 °C, which indicated that the ODS FeCrAl alloy is capable of accident-tolerant fuel (ATF) clad material [52]. Further, Sakamoto, Miura, Ukai, et al. [53] conducted reaction tests between ODS FeCrAl and UO_2 in an inert gas atmosphere at 1723 K for 25 h. The Al_2O_3 scale with a thickness of 3.6 μm was formed, and no detectable inter-diffusion across the oxide scale was found, as shown in **Figure 7**. More research [62] showed that the growth rate of the Al_2O_3 reaction layer of the FeCrAlZr-ODS with UO_2 was evaluated to be 10^{-8}–10^{-7} m^2 s^{-1}, while the rate of the reaction layer between zircaloy and UO_2 was extremely large at the same temperature (10^{-2}–10^{-1} m^2 s^{-1}), indicating good compatibility.

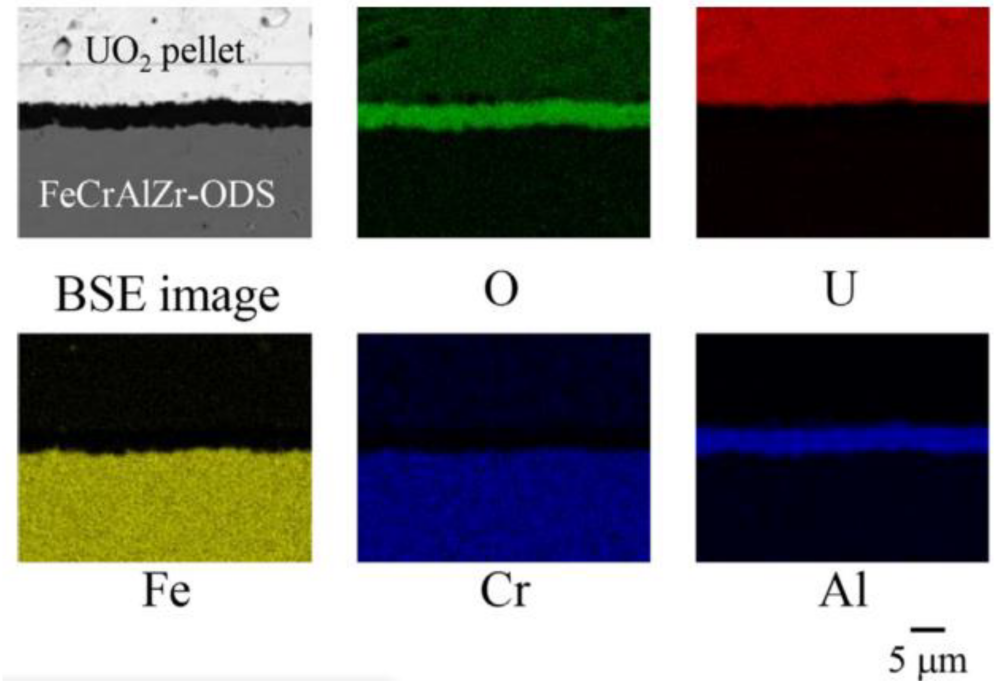

Figure 7. Elemental mappings on the cross-section of the reaction couple of FeCrAlZr–ODS–UO_2 at 1723 K for 25 h.

2.2.2. Low Temperature Corrosion in a Light Water Nuclear Reactor (T < 1000 °C)

The normal operating temperature in II and III Generation light water nuclear reactors ranges from 290 to 320 °C, while in the IV generation of supercritical pressurized water reactor (SCW), the operating temperature increases from 290 to 600 °C. Therefore, the corrosion behavior of the ODS FeCrAl alloy in the lower temperature range of 200–700 °C over the long term has also been widely studied. Isselin et al. [63] compared the corrosion behavior of 16Cr–4Al ODS and 16 Cr ODS steel in a SCW environment (pure water, 25 MPa, 8 ppm) at 550 °C and found that the addition of 4 wt.% Al can effectively improve corrosion resistance. A dense protective layer of Al_2O_3 is formed on the surface of 16Cr–4Al ODS, while (Cr, Fe)$_2O_3$ is formed on the surface of 16 Cr ODS steel. Lee et al. [64] studied systematically the corrosion behavior of ODS steel doped with various alloy elements, such as Cr, Al, W, Ce, Hf, and Zr, in SCW (25 MPa and 8 ppm dissolved oxygen) at different temperatures of 400, 500, and 600 °C. The research revealed that the addition and content of different chemical elements lead to different corrosion products resulting from different corrosion mechanisms, as shown in **Figure 8**, and Al addition led to a dense protective layer of Al_2O_3 among complex corrosion products. It was also found that the thickness of the oxide layer is also closely related to the exposure temperature and time, which is due to the different diffusion coefficients of the O atoms at different temperatures. The resistance to corrosion at low temperatures also depends on the content of the Al element. For example, exposed to SCW at 600 °C for one year, the oxide thickness of SOC-1 (with a higher Al of 3.5 wt.%) was only 5 μm. It showed that 4 wt.% Al addition can effectively improve the corrosion resistance of 16Cr–ODS, and the appropriate composition ratio of Cr and Al is in the range of (14–16) Cr and (3.5–4.5) Al for SCW application. Briefly, in SCW, it can be seen that Al addition and content strongly control the corrosion rate, corrosion products, and corrosion mechanism of the alloy.

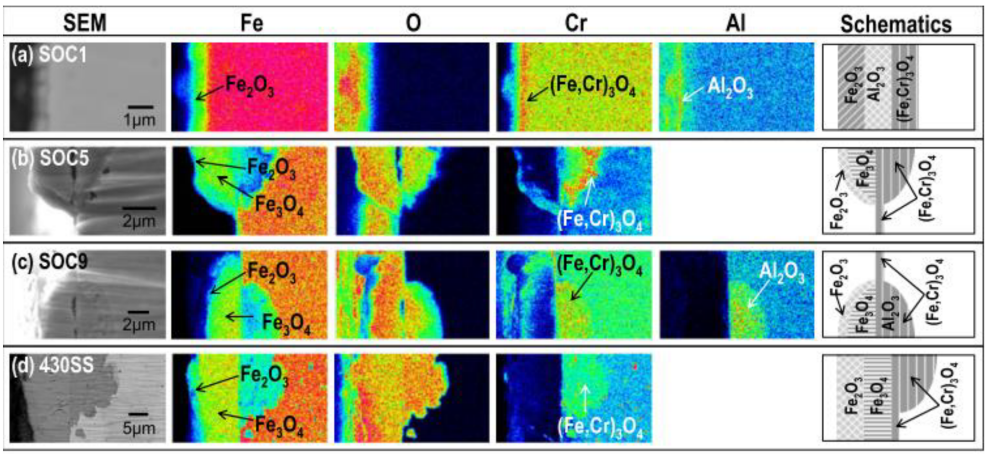

Figure 8. SEM images showing the cross-sectional morphologies of (**a**) SOC-1 (Fe–16.11Cr–3.44Al–0.09Ti–0.34Y_2O_3), (**b**) SOC-5 (Fe–15.95Cr–0.09Ti–0.34Y_2O_3), (**c**) SOC-9 (Fe–15.42Cr–1.85W–3.8Al–0.10Ti–0.36Y_2O_3), and (**d**) type 430 SS (Fe–16Cr) and FE-EPMA analyses showing the corresponding composition distributions after exposure at 500 °C.

Ren et al. [65] systematically investigated the effect of corrosion time (200, 400, 600, 800, and 1000 h) on the corrosion behavior of the 16Cr–3Al ODS alloy in SCW at 600 °C. It is concluded that with the extension of corrosion time, the thickness of the oxide layer and weight gain agree with the parabolic law in the case of the types of corrosion products without changing. On the basis of these results, the corrosion mechanism under this experimental condition was discussed in detail, as schematically shown in **Figure 9**. Simply put, the lower standard Gibbs free energy [66] of Al_2O_3 compared with Cr_2O_3 and Fe_2O_3, the difference in concentration of the elements in the alloy, the chemical gradient, and the difference in the ion diffusion coefficient make it form a double-layer oxide structure with Al_2O_3 as the inner oxide layer and $(Cr, Fe)_2O_3$ as the outer oxide layer. Finally, due to the densification of Al_2O_3 and the low diffusion coefficient [67] of Fe and Cr in Al_2O_3, the outward diffusion of Cr^{3+} and Fe^{3+} was obviously limited, and the growth of the outer oxide layer slowed. Under the circumstances, the process of oxidation became stable as a result of the protection of the compact internal Al_2O_3 layer, resulting in the prevention of corrosion damage.

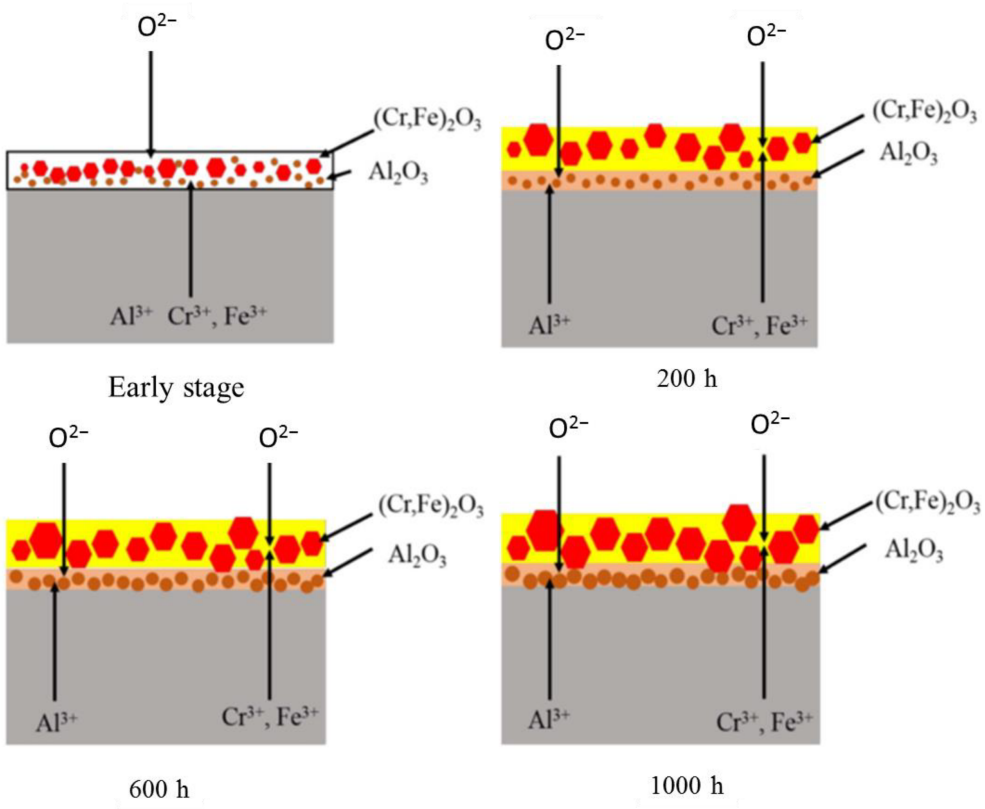

Figure 9. Schematic representation of the microstructural evolution of the oxide layer at an early stage in SCW and after exposure for 200 h, 600 h, and 1000 h, respectively.

In ORNL of the United States, Terrani et al. [68][69] conducted the corrosion test for several low Cr FeCrAl alloys in water with three different chemical composition environments (found in the main cooling cycle conditions of PWR and BWR) for up to one year in a temperature range of 290–330 °C. The maximum thickness loss of LWR corrosion for one year without irradiation is 2 μm, which can be ignored for cladding with 300–500 μm thickness in actual application. Recently, a corrosion resistance test for a second generation of several FeCrAl alloys was conducted in simulated BWR-HWC and BWR-NWC under normal operating conditions [69]. The thickness of the

oxide layer on Fe–10Cr–6Al increased most slowly after exposure to the corrosive environment of BWR-HWC (as shown in **Figure 10**) and exhibited satisfactory corrosion resistance in the corrosive environment of BWR-NWC.

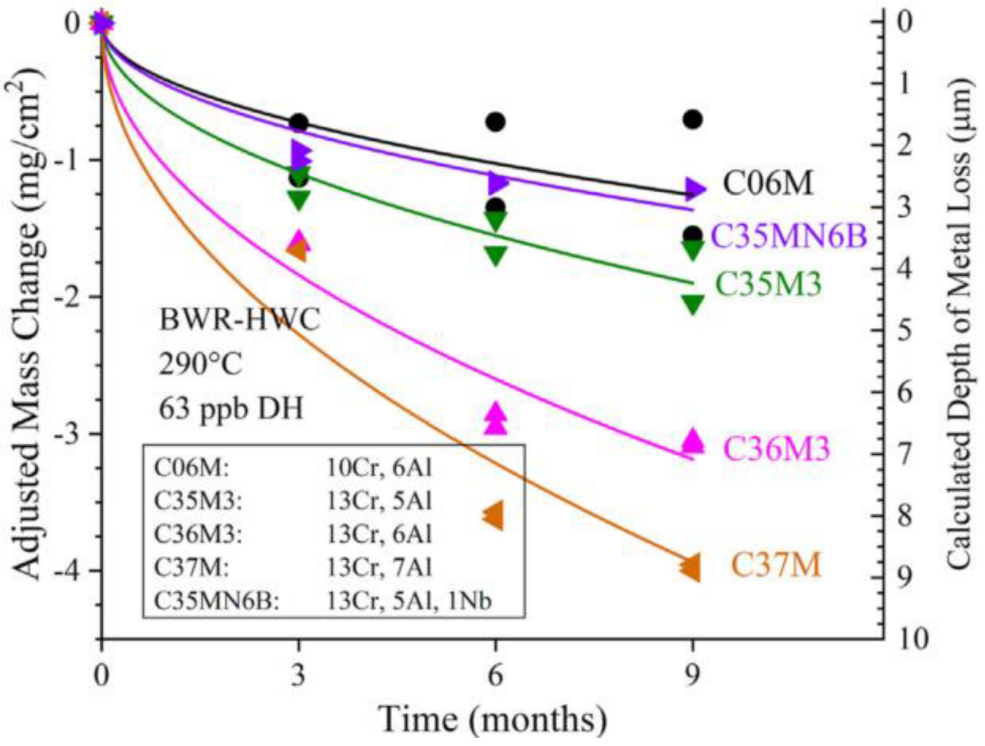

Figure 10. Adjusted mass change of 2nd generation FeCrAl alloys exposed to BWR-HWC (290 °C, 62 wppb DH) with fitted curves.

2.2.3. Compatibility with Liquid Metal Medium

Al plays a critical role in the corrosion resistance of candidate alloys in liquid metal. There exists a contradictory fact that Ni/Fe/Cr elements are very important in austenitic stainless/ferrite steel, but lead–bismuth eutectics (LBE) have high solubility for the above three elements. So, Ni superalloy and Fe–based austenitic stainless steel are difficult to utilize as structural materials for the LBE cooling system, especially above 773 K. Above 873 K, the solubility/corrosion of Fe and Cr in LBE increase remarkably. In order to keep the material from dissolving in LBE, the Al_2O_3 layers that form on the surface of the Al-containing steel are considered to inhibit the dissolution. **Figure 11** shows ODS samples under certain LBE conditions (10^{-6} wt.% O_2 in solution for 10^4 h at 923 K). The 19Cr–ODS steel without Al dissolves significantly in LBE. However, the ODS samples with 4 wt.% Al retain almost completely their shape, indicating high corrosion resistance. It should be noted that with the same Al content, the change in Cr content (13–19 wt.%) does not have a remarkable impact on the corrosion resistance of the alloys in LBE [28].

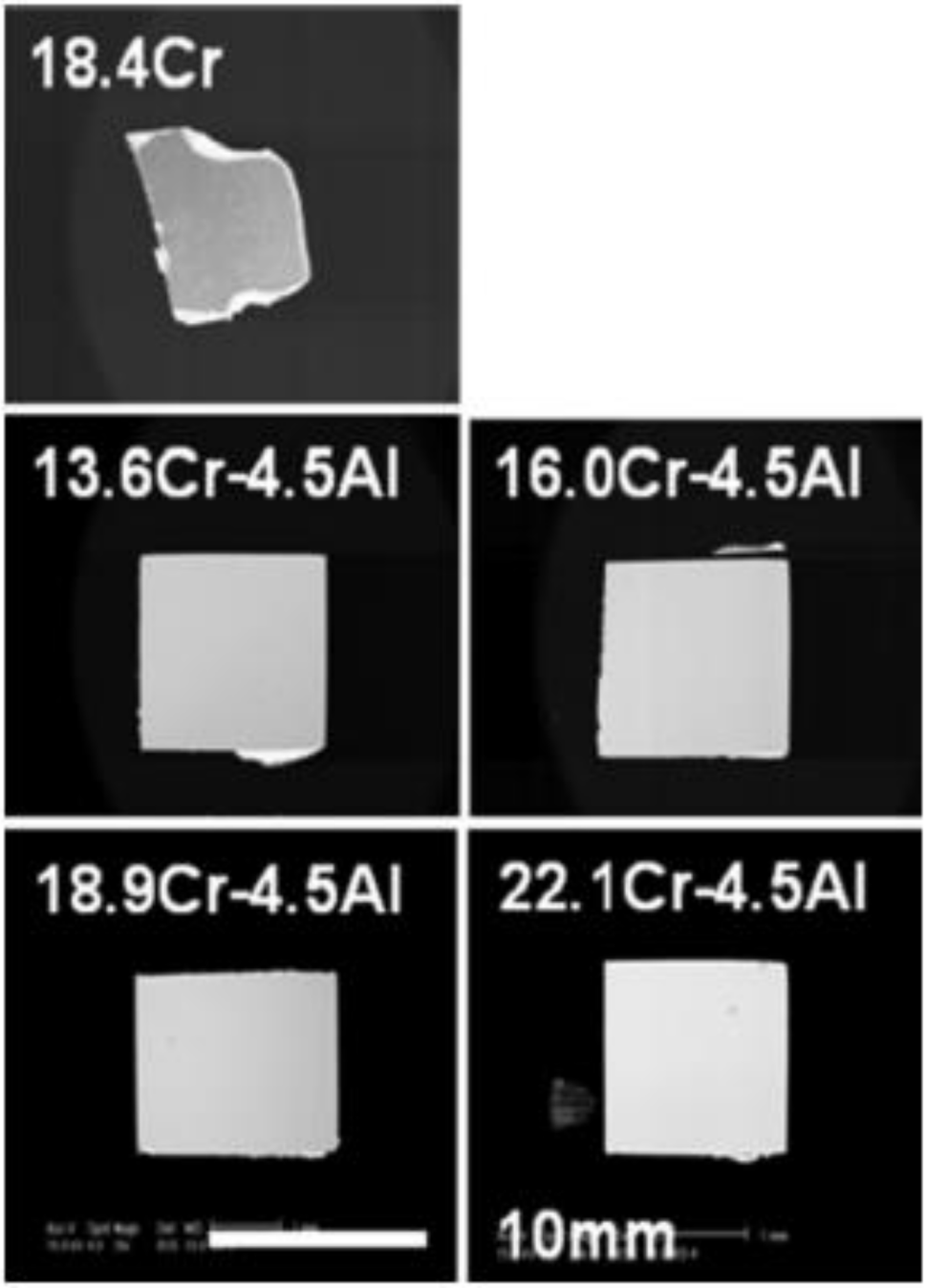

Figure 11. The appearance of ODS steel specimens after corrosion tests in LBE solved with 10^{-6} wt.% for 1×10^4 h at 923 K.

Hosemann et al. [70] compared the corrosion resistance of five different ODS experimental and commercial alloys, including Fe–Cr ferritic/martensitic steels (12YWT, 14YWT, and MA957) and FeCrAl alloys (PM2000 and MA956), under the conditions of liquid lead–bismuth eutectic at 535 °C for 200 h and 600 h. The results showed that PM2000 with an Al content greater than 5.5 wt.% exhibits good corrosion/oxidation resistance, which is closely related to grain size. Takaya et al. [71] systematically studied the corrosion resistance of ODS steel with an Al content of 0–3.5 wt.% and a Cr content of 13.7–17.3 wt.% and a 12Cr steel. The results showed that when the Al content is 3.5 wt.% and the Cr content is 13.7–17.3 wt.%, a protective Al oxide layer can be formed on the surface

of ODS steel, while increasing the Cr concentration alone cannot improve the corrosion resistance. These research conclusions show that Al plays a decisive role in the corrosion resistance of the alloy in the lead–bismuth eutectic environment.

Regarding Pb-Li compatibility in the fusion reactor, Unocic et al. [72] exposed model FeCrAlY alloys with 10–20 wt.% Cr and 3–5 wt.% Al for 1000 h at 700 °C. The results showed that the effect of Cr content on mass change was not obvious; however, mass losses happened to alloys with <5 wt.% Al in these experiments, indicating that Al plays a more important role than Cr in the Pb–Li coolant. The corrosion experiment for the first generation of low Cr ODS FeCrAl (based on Fe–12Cr–5Al) developed by the Oak Ridge National Laboratory [58][59][73] has been completed at 700 °C. It showed that the Pb–Li compatibility of the ODS FeCrAl alloys is better than that of the wrought FeCrAl and ODS Fe–Cr alloys (**Figure 12**). A thin (~1 μm) $LiAlO_2$ reaction product was detected in all cases (**Figure 13**), indicating that the corrosion resistance of low Cr ODS FeCrAl meets the service requirements of the liquid lead–bismuth eutectic reactor.

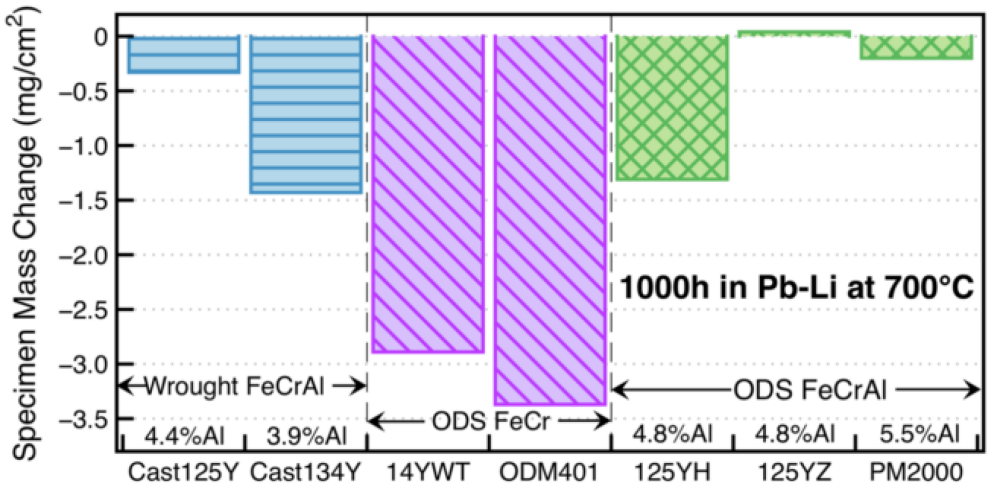

Figure 12. Specimen mass change for alloy specimens exposed for 1000 h at 700 °C in static PbLi.

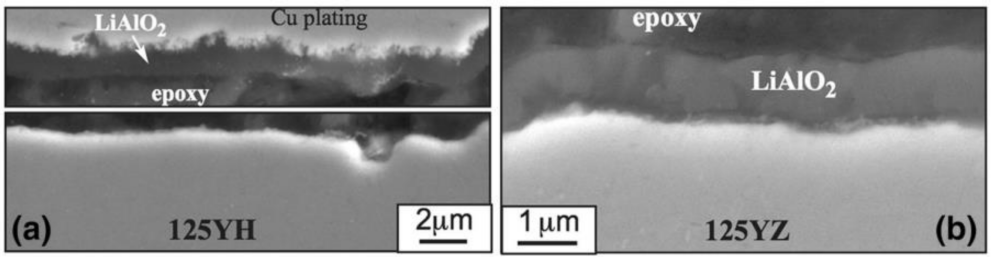

Figure 13. SEM backscattered electron images of polished cross-sections after 1000 h in Pb–Li at 700 °C of (**a**) 125YH and (**b**) 125YZ. In (**a**), the oxide delaminated during specimen preparation.

The historical evolution of the development of the ODS FeCrAl alloy summarized above shows that the low Cr and high Al ODS FeCrAl alloy with a certain ratio has excellent application prospects in the light water-cooling medium (fission reactor) or metal cooling medium (fission/fusion reactor) from the perspective of corrosion resistance.

2.2.4. Effect of Al on Strength and Workability

The addition of Al has a significant effect on the dispersed oxides and mechanical properties of ODS steel [74]. For example, Kasada et al. [75] studied the microstructure and tensile properties of oxidation dispersion strengthened (ODS) ferritic steels K1 (F–19Cr–0.3W–0.3Ti–0.3Y_2O_3) and K4 (Fe–19Cr–4Al–2W–0.3Ti–0.3Y_2O_3) before and after deformation. The nano-oxides in K1 were cubic chlore $Y_2Ti_2O_7$, and the nano-oxides in K4 were mainly perovskite $YAlO_3$ with a larger size than $Y_2Ti_2O_7$, which indicated that the addition of Al changed the type and average size of the ODS particles and resulted in a much higher strength of K1 (Al-free) than that of K4 (Al-containing). In similar studies, Gong et al. [76] prepared two ODS ferritic alloys with compositions (wt.%) of Fe–14Cr–4.5Al–1W–0.35Y_2O_3 (14Cr–Al ODS) and Fe–14Cr–0.5Ti–1W–0.35Y_2O_3 (14Cr–Ti ODS) by mechanical alloying and hot isostatic pressing. Tensile tests showed that 14Cr–Ti ODS steel has higher strength but weaker ductility, while 14Cr–Al ODS alloy has lower strength but better ductility. In addition, 14Cr–Al ODS alloy shows a higher impact energy than that of 14Cr–Ti ODS alloy. A similar behavior in mechanical properties was reported in references [28][77][78].

Except for a reduction in tensile strength due to the addition of Al, the higher Al content increases the difficulty of welding and manufacturing [79][80][81] and increases the brittleness of the alloy simultaneously [82][83]. Moreover, investigation [84] revealed that ordered Fe_3Al intermetallic phase precipitating during aging increases the strength and decreases the ductility of aged ODS FeCrAl ferritic alloys when the amount of Al exceeds 10 wt.%. Thus, the upper limit of Al that can be safely added to ODS FeCrAl ferritic alloys for accident-tolerant fuel cladding is on the order of 7~8 wt.%. Thus, it can be concluded that these experimental data provide the basis for the maximum amount of Al addition in the processing or service of the alloy. In addition, it should be noted that when ODS FeCrAl alloys are exposed to oxygen and air at 1000–1300 °C, Al depletion will occur in the matrix. Therefore, the change in the Al concentration in the matrix can determine the service life of these alloys; that is, when the aluminum content is less than a critical value, the oxidation resistance of the alloys is limited. The protective layer of alumina can no longer heal, so the matrix oxide products are rapidly formed, which results in rapid consumption of materials. This phenomenon is called “separation oxidation”, which corresponds to the end of material life. When scale peeling occurs, especially in the thermal cycle, this phenomenon will accelerate [85]. This phenomenon of “separation oxidation” should be avoided during thermal mechanical processing because it may make the material unable to meet the corrosion resistance requirements and fail in normal service or accident situations.

References

1. Zinkle, S.J.; Terrani, K.A.; Gehin, J.C.; Ott, L.J.; Snead, L.L. Accident tolerant fuels for LWRs: A perspective. J. Nucl. Mater. 2014, 448, 374–379.
2. Department of Energy. Development of Light Water Reactor Fuels with Enhanced Accident Tolerance. In Report to Congress; Department of Energy: Washington, DC, USA, 2015.

3. Rebak, R.B.; Andresen, P.L.; Kim, Y.J.; Dolley, E.J. Characterization of Advanced Steels as Accident Tolerant Fuel Cladding for Light Water Reactors; Technical Report IAEA-TECDOC-1797; International Atomic Energy Agency: Vienna, Austria, 2014.
4. Rebak, R.B. Characterization of Advanced Steels as Accident Tolerant Cladding for Light Water Reactor Nuclear Fuel. In Proceedings of the ASME 2015 Pressure Vessels and Piping Conference, Boston, MA, USA, 19–23 July 2015.
5. Rebak, R.B. Alloy selection for accident tolerant fuel cladding in commercial light water reactors. Metall. Mater. Trans. E 2015, 2, 197–207.
6. Rebak, R.B.; Terrani, K.A.; Fawcett, R.M. FeCrAl Alloys for Accident Tolerant Fuel Cladding in Light Water Reactors. In Proceedings of the ASME 2016 Pressure Vessel & Piping Conference, Vancouver, BC, Canada, 17–21 July 2016.
7. Rebak, R.B.; Larsen, M.; Kim, Y.J. Characterization of oxides formed on iron-chromium-aluminum alloy in simulated light water reactor environments. Corros. Rev. 2017, 35, 177–188.
8. Rebak, R.B.; Terrani, K.A.; Gassmann, W.P.; Williams, J.B.; Ledford, K.L. Improving nuclear power plant safety with FeCrAl alloy fuel cladding. MRS Adv. 2017, 2, 1217–1224.
9. Dolley, E.J.; Schuster, M.; Crawford, C.; Rebak, R.B. Mechanical behavior of FeCrAl and other alloys following exposure to LOCA conditions plus quenching. In Proceedings of the 18th International Conference on Environmental Degradation of Materials in Nuclear Power Systems—Water Reactors, Portland, OR, USA, 13–17 August 2017; Springer: Cham, Switzerland, 2018; pp. 185–200.
10. Tortorelli, P.F.; Brady, M.P. Alloy design approaches for high-temperature oxidation resistance. JOM 2000, 52, 15.
11. Terrani, K.A. Accident tolerant fuel cladding development: Promise, status, and challenges. J. Nucl. Mater. 2018, 501, 13–30.
12. Opila, E.J.; Jacobson, N.S.; Myers, D.L.; Copland, E.H. Predicting oxide stability in high-temperature water vapor. JOM 2006, 58, 22–28.
13. Cheng, T.; Keiser, J.R.; Brady, M.P.; Terrani, K.A.; Pint, B.A. Oxidation of fuel cladding candidate materials in steam environments at high temperature and pressure. J. Nucl. Mater. 2012, 427, 396–400.
14. Miller, M.K.; Russell, K.F.; Hoelzer, D.T. Characterization of precipitates in MA/ODS ferritic alloys. J. Nucl. Mater. 2006, 351, 261–268.
15. Alinger, M.J.; Odette, G.R.; Hoelzer, D.T. On the role of alloy composition and processing parameters in nanocluster formation and dispersion strengthening in nanostuctured ferritic alloys. Acta Mater. 2009, 57, 392–406.

16. Miller, M.K.; Reinhard, D.; Larson, D.J. Detection and quantification of solute clusters in a nanostructured ferritic alloy. J. Nucl. Mater. 2015, 462, 428–432.
17. Ohtsuka, S.; Ukai, S.; Fujiwara, M. Nano-mesoscopic structural control in 9CrODS ferritic/martensitic steels. J. Nucl. Mater. 2006, 351, 241–246.
18. Odette, G.R.; Alinger, M.J.; Wirth, B.D. Recent Developments in Irradiation-Resistant Steels. Annu. Rev. Mater. Res. 2008, 38, 471–503.
19. Ukai, S.; Mizuta, S.; Fujiwara, M.; Okuda, T.; Kobayashi, T. Development of 9Cr-ODS martensitic steel claddings for fuel pins by means of Ferrite to Austenite phase transformation. J. Nucl. Sci. Technol. 2002, 39, 778–788.
20. Ohtsuka, S.; Shizukawa, Y.; Tanno, T.; Imagawa, Y.; Hashidate, R.; Yano, Y.; Onizawa, T.; Kaito, T.; Ohnuma, M.; Mitsuhara, M.; et al. High-temperature creep properties of 9Cr- ODS tempered martensitic steel and quantitative correlation with its nanometer- scale structure. J. Nucl. Sci. Technol. 2023, 60, 288–298.
21. Zinkle, S.J.; Boutard, J.L.; Hoelzer, D.T.; Kimura, A.; Lindau, R.; Odette, G.R.; Rieth, M.; Tan, L.; Tanigawa, H. Development of next generation tempered and ODS reduced activation ferritic/martensitic steels for fusion energy applications. Nucl. Fusion 2017, 57, 092005.
22. Odette, G.R. On the status and prospects for nanostructured ferritic alloys for nuclear fission and fusion application with emphasis on the underlying science. Scr. Mater. 2018, 143, 142–148.
23. Wharry, J.P.; Swenson, M.J.; Yano, K.H. A review of the irradiation evolution of dispersed oxide nanoparticles in the b. c. c. Fe-Cr system: Current understanding and future directions. J. Nucl. Mater. 2017, 486, 11–20.
24. Azeem, M.M.; Li, Z.; Wang, Q.; Zubair, M. Molecular dynamics studies and irradiation effects in ODSS alloys. Int. J. Nucl. Energy Sci. Technol. 2019, 12, 381–399.
25. Mustafa Azeem, M.; Wang, Q.Y.; Li, Z.Y.; Zhang, Y. Dislocation-oxide interaction in Y2O3 embedded Fe: A molecular dynamics simulation study. Nucl. Eng. Technol. 2020, 52, 337–343.
26. Locatelli, G.; Mancini, M.; Todeschini, N. Generation IV nuclear reactors: Current status and future prospects. Energy Policy 2013, 61, 1503–1520.
27. Abram, T.; Ion, S. Generation–IV nuclear power: A review of the state of the science. Energy Policy 2008, 36, 4323–4330.
28. Kimura, A.; Kasada, R.; Iwata, N.; Kishimoto, H.; Zhang, C.H.; Isselin, J.; Dou, P.; Lee, J.H.; Muthukumar, N.; Okuda, T.; et al. Development of Al added high—Cr ODS steels for fuel cladding of next generation nuclear systems. J. Nucl. Mater. 2011, 417, 176–179.
29. Pint, B.A.; Wright, I.G. Long-term high temperature oxidation behavior of ODS ferritics. J. Nucl. Mater. 2002, 307–311, 763–768.

30. Pint, B.A.; Wright, I.G. Oxidation behavior of ODS Fe-Cr alloys. Oxid. Met. 2005, 63, 193–213.
31. Kimura, A.; Cho, H.S.; Toda, N.; Kasada, R.; Yutani, K.; Kishimoto, H.; Iwata, N.; Ukai, S.; Fujiwara, M. High Burnup Fuel Cladding Materials R&D for Advanced Nuclear Systems: Nano-sized oxide dispersion strengthening steels. J. Nucl. Sci. Technol. 2007, 44, 323–328.
32. Cho, H.S.; Kimura, A. Corrosion resistance of high-Cr oxide dispersion strengthened ferritic steels in super-critical pressurized water. J. Nucl. Mater. 2007, 367–370, 1180–1184.
33. Capdevila, C.; Miller, M.K.; Chao, J. Phase separation kinetics in a Fe-Cr-Al alloy. Acta Mater. 2012, 60, 4673–4684.
34. Capdevila, C.; Miller, M.K.; Toda, I.; Chao, J. Influence of the a-a'phase separation on the tensile properties of Fe-base ODS PM2000 alloy. Mater. Sci. Eng. 2010, 527, 7931–7938.
35. Terada, M.; Hupalo, M.F.; Costa, I.; Padilha, A.F. Effect of alpha prime due to 475 °C aging on fracture behavior and corrosion resistance of DIN 1.4575 and MA 956 high performance ferritic stainless steels. J. Mater. Sci. 2008, 43, 425–433.
36. Dryepondt, S.; Unocic, K.A.; Hoelzer, D.T.; Massey, C.P.; Pint, B.A. Development of low-Cr ODS FeCrAl alloys for accident-tolerant fuel. J. Nucl. Mater. 2018, 501, 59–71.
37. Lee, J.S.; Jang, C.H.; Kim, I.S.; Kimura, A. Embrittlement and hardening during thermal aging of high Cr oxide dispersion strengthened alloys. J. Nucl. Mater. 2007, 367–370, 229–233.
38. Field, K.G.; Hu, X.; Littrell, K.C.; Yamamoto, Y.; Snead, L.L. Radiation tolerance of neutron-irradiated model Fe-Cr-Al alloys. J. Nucl. Mater. 2015, 465, 746–755.
39. Briggs, S.A.; Edmondson, P.D.; Littrell, K.C.; Yamamoto, Y.; Howard, R.H.; Daily, C.R.; Terrani, K.A.; Sridharan, K.; Field, K.G. A combined APT and SANS investigation of a' phase precipitation in neutron-irradiated model FeCrAl alloys. Acta Mater. 2017, 129, 217–228.
40. Li, S.; Zhou, Z.; Jang, J.; Wang, M.; Hu, H.; Sun, H.; Zou, L.; Zhang, G.; Zhang, L. The influence of Cr content on the mechanical properties of ODS ferritic steels. J. Nucl. Mater. 2014, 455, 194–200.
41. Noh, S.; Choi, J.E.; Choi, B.K.; Kang, S.H.; Kim, T.K. Effects of Cr, Mo, Al, Zr, Y2O3 on the microstructures and tensile properties of ODS ferritic/martensitic alloys. J. Met. Mater. 2014, 52, 705–712.
42. Bachhav, M.; Odette, G.R.; Marquis, E.A. Microstructural Changes in a Neutron-Irradiated Fe-15 at. % Cr Alloy. J. Nucl. Mater. 2014, 454, 381–386.
43. Pawel, J.E.; Rowcliffe, A.F.; Lucas, G.E.; Zinkle, S.J. Irradiation Performance of Stainless Steels for ITER Application. J. Nucl. Mater. 1996, 239, 126–131.

44. Tanigawa, H.; Shiba, K.; Möslang, A.; Stoller, R.E.; Lindau, R.; Sokolov, M.A.; Odette, G.R.; Kurtz, R.J.; Jitsukawa, S. Status and key issues of reduced activation ferritic/martensitic steels as the structural material for a DEMO blanket. J. Nucl. Mater. 2011, 417, 9–15.
45. Niu, Y.; Wang, S.; Gao, F.; Zhang, Z.G.; Gesmundo, F. The nature of the third- element effect in the oxidation of Fe-xCr-3at.%Al alloys in 1 atm O2 at 1000 °C. Corros. Sci. 2008, 50, 345–356.
46. Stott, F.H.; Wood, G.C.; Stringer, J. The Influence of Alloying Elements on the Development and Maintenance of Protective Scales. Oxid. Met. 1995, 44, 113–145.
47. Kobayashi, S.; Takasugi, T. Mapping of 475 °C embrittlement in ferritic Fe–Cr–Al alloys. Scr. Mater. 2010, 63, 1104–1107.
48. Li, W.; Lu, S.; Hu, Q.M.; Mao, H.H.; Johansson, B.; Vitos, L. The effect of Al on the 475 °C embrittlement of Fe-Cr alloys. Comp. Mater. Sci. 2013, 74, 101–106.
49. Han, W.T.; Yabuuchi, K.; Kimura, A.; Ukai, S.; Oono, N.; Kaito, T.; Torimaru, T.; Hayashi, S. Effect of Cr/Al contents on the 475 °C age-hardening in oxide dispersion strengthened ferritic steels. Nucl. Mater. Energy 2016, 9, 610–615.
50. Field, K.G.; Littrell, K.C.; Briggs, S.A. Precipitation of α′ in neutron irradiated commercial FeCrAl alloys. Scr. Mater. 2018, 142, 41–45.
51. Yang, Z.; Wang, Z.X.; Xia, C.H.; Ouyang, M.H.; Peng, J.C.; Zhang, H.W.; Xiao, X.S. Aluminum suppression of α′ precipitate in model Fe–Cr–Al alloys during long-term aging at 475 °C. Mater. Sci. Eng. A 2020, 772, 138714.
52. Maeda, T.; Ukai, S.; Hayashi, S.; Oono, N.; Shizukawa, Y.; Sakamoto, K. Effects of zirconium and oxygen on the oxidation of FeCrAl-ODS alloys under air and steam conditions up to 1500 °C. J. Nucl. Mater. 2019, 516, 317–326.
53. Sakamoto, K.; Miura, Y.; Ukai, S.; Oono, N.H.; Kimura, A.; Yamaji, A.; Kusagaya, K.; Takano, S.; Kondo, T.; Ikegawa, T.; et al. Development of accident tolerant FeCrAl-ODS fuel cladding for BWRs in Japan. J. Nucl. Mater. 2021, 557, 153276.
54. Liu, T.; Wang, C.X.; Shen, H.L.; Chou, W.S.; Iwata, N.Y.; Kimura, A. The effects of Cr and Al concentrations on the oxidation behavior of oxide dispersion strengthened ferritic alloys. Corros. Sci. 2013, 76, 310–316.
55. Liu, T.; Wang, L.B.; Wang, C.X.; Shen, H.L. Effect of Al content on the oxidation behavior of Y2Ti2O7-dispersed Fe-14Cr ferritic alloys. Corros Sci. 2016, 104, 17–25.
56. Weisenburger, A.; Jianu, A.; Doyle, S.; Bruns, M.; Fetzer, R.; Heinzel, A.; Del Giacco, M.; An, W.; Muller, G. Oxide scales formed on Fe—Cr—Al—Based model alloys exposed to oxygen containing molten lead. J. Nucl. Mater. 2013, 437, 282–292.

57. Tomaszewicz, P.; Wallwork, G.R. The oxidation of high-purity iron-chromium-aluminum alloys at 800 °C. Oxid. Met. 1983, 20, 75–109.
58. Pint, B.A.; Dryepondt, S.; Unocic, K.A.; Hoelzer, D.T. Development of ODS FeCrAl for compatibility in fusion and fission energy applications. JOM 2014, 66, 2458–2466.
59. Unocic, K.A.; Hoelzer, D.T.; Pint, B.A. Microstructure and environmental resistance of low Cr ODS FeCrAl. Mater. High Temp. 2015, 32, 123–132.
60. Dryepondt, S.; Massey, C.; Edmonson, P.D. 2nd Generation ODS FeCrAl Alloy Development for Accident-Tolerant Fuel Cladding; ORNL/TM—2016/456; National Technical Information Service: Springfield, VA, USA, 2016.
61. Qiao, Y.J.; Wang, P.; Qi, W.; Du, S.Y.; Liu, Z.; Meng, F.P.; Zhang, X.H.; Wang, K.; Li, Q.W.; Yao, Z.D.; et al. Mechanism of Al on FeCrAl steam oxidation behavior and molecular dynamics simulations. J. Alloys Compd. 2020, 828, 154310.
62. Hofmann, P. Current knowledge on core degradation phenomena, a review. J. Nucl. Mater. 1999, 270, 194–211.
63. Isselin, J.; Kasada, R.; Kimura, A. Corrosion behaviour of 16% Cr—4% Al and 16% Cr ODS ferritic steels under different metallurgical conditions in a supercritical water environment. Corros. Sci. 2010, 52, 3266–3270.
64. Lee, J.H.; Kasada, R.; Kimura, A.; Okudab, T.; Inoue, M.; Ukai, S.; Ohnuki, S.; Fujisawa, T.; Abef, F. Influence of alloy composition and temperature on corrosion behavior of ODS ferritic steels. J. Nucl. Mater. 2011, 417, 1225–1228.
65. Ren, J.; Yu, L.M.; Liu, Y.C.; Ma, Z.Q.; Liu, C.X.; Li, H.J.; Wu, J.F. Corrosion behavior of an Al added high-Cr ODS steel in supercritical water at 600 °C. Appl. Surf. Sci. 2019, 480, 969–978.
66. Huttunen-Saarivirta, E.; Kuokkala, V.T.; Pohjanne, P. Thermally grown oxide films and corrosion performance of ferritic stainless steels under simulated exhaust gas condensate conditions. Corros. Sci. 2014, 87, 344–365.
67. Liu, Y.C.; Chen, S.M.; Ouyang, F.Y.; Kai, J.J. Corrosion behavior of pre-oxidized HR—224 superalloy in supercritical water environment at 700 °C. J. Nucl. Mater. 2018, 505, 7–14.
68. Terrani, K.A.; Pint, B.A.; Kim, Y.J.; Unocic, K.A.; Yang, Y.; Silva, C.M.; Meyer, H.M.; Rebak, R.B. Uniform corrosion of FeCrAl alloys in LWR coolant environments. J. Nucl. Mater. 2016, 479, 36–47.
69. Raiman, S.S.; Field, K.G.; Rebak, R.B.; Yamamoto, Y.; Terrani, K.A. Hydrothermal corrosion of 2nd generation FeCrAl alloys for accident tolerant fuel cladding. J. Nucl. Mater. 2020, 536, 152221.

70. Hosemann, P.; Thau, H.T.; Johnson, A.L.; Maloy, S.A.; Li, N. Corrosion of ODS steels in lead—Bismuth eutectic. J. Nucl. Mater. 2008, 373, 246–253.
71. Takaya, S.; Furukawa, T.; Aoto, K.; Müller, G.; Weisenburger, A.; Heinzel, A.; Inoue, M.; Okudac, T.; Abed, F.; Ohnuki, S.; et al. Corrosion behavior of Al—Alloying high Cr—ODS steels in lead-bismuth eutectic. J. Nucl. Mater. 2009, 386–388, 507–510.
72. Unocic, K.A.; Pint, B.A. Alloying and coating strategies for improved Pb—Li compatibility in DEMO—Type fusion reactors. J. Nucl. Mater. 2014, 455, 330.
73. Unocic, K.A.; Hoelzer, D.T. Evaluation of Pb—17Li compatibility of ODS Fe-12Cr-5Al alloys. J. Nucl. Mater. 2016, 479, 357–364.
74. Klueh, R.L.; Shingledecker, J.P.; Swindeman, R.W.; Hoelzer, D.T. Oxide dispersion-strengthened steels: A comparison of some commercial and experimental alloys. J. Nucl. Mater. 2005, 341, 103–114.
75. Kasada, R.; Toda, N.; Yutani, K.; Cho, H.S.; Kishimoto, H.; Kimura, A. Pre- and post-deformation microstructures of oxide dispersion strengthened ferritic steels. J. Nucl. Mater. 2007, 367–370, 222–228.
76. Gong, M.; Zhou, Z.; Hu, H.; Zhang, G.; Li, S.; Wang, M. Effects of Aluminum on Microstructure and Mechanical Behavior of 14Cr—ODS Steels. J. Nucl. Mater. 2015, 462, 502–507.
77. Lee, J.H. Development of oxide dispersion strengthened ferritic steels with and without aluminum. Front. Energy 2012, 6, 29–34.
78. Zhang, G.; Zhou, Z.; Mo, K.; Miao, Y.; Li, S.; Liu, X.; Wang, M.; Park, J.S.; Almer, J.; Stubbins, J.F. The comparison of microstructures and mechanical properties between 14Cr—Al and 14Cr—Ti ferritic ODS alloys. Mater. Des. 2016, 98, 61–67.
79. Gussev, M.N.; Field, K.G.; Yamamoto, Y. Design, properties and weldability of advanced oxidation-resistant FeCrAl alloys. Mater. Des. 2017, 129, 227–238.
80. Capdevila, C.; Miller, M.K.; Russell, K.F. Aluminum partitioning during phase separation in Fe—20%Cr-6%Al ODS alloy. J. Mater. Sci. 2008, 43, 3889–3893.
81. Vicente, A.D.A.; Moreno, J.R.S.; Espinosa, D.C.R.; Santos, T.F.D.A.; Tenorio, J.A.S. Study of the high temperature oxidation and Kirkendall porosity in dissimilar welding joints between Fe—Cr—Al alloy and stainless steel AISI 310 after isothermal heat treatment at 1150 °C in air. J. Mater. Res. Technol. 2019, 8, 1636–1644.
82. Wukusick, C.S.; Collis, J.F. An Iron—Chromium—Aluminum Alloy Containing Yttrium. Mater. Res. Stand. 1964, 12, 637–646.
83. Xu, S.; Zhou, Z.J.; Long, F.; Jia, H.D.; Guo, N.; Yao, Z.W.; Daymond, M.R. Combination of back stress strengthening and Orowan strengthening in bimodal structured Fe—9Cr—Al ODS steel

with high Al addition. Mater. Sci. Eng. A 2019, 739, 45–52.

84. Maji, B.C.; Ukai, S.; Oono, N. Microstructural stability and intermetallic embrittlement in high Al containing FeCrAl—ODS alloys. Mater. Sci. Eng. A 2021, 807, 140858.
85. Maréchal, L.; Lesage, B.; Huntz, A.M.; Molins, R. Oxidation Behavior of ODS Fe—Cr—Al Alloys: Aluminum Depletion and Lifetime. Oxid. Met. 2003, 60, 1–28.